ANL/NSE-19/9

Development of Heat Pipe Reactor Modeling in SAM

Nuclear Science and Engineering Division

About Argonne National Laboratory
Argonne is a U.S. Department of Energy laboratory managed by UChicago Argonne, LLC under contract DE-AC02-06CH11357. The Laboratory's main facility is outside Chicago, at 9700 South Cass Avenue, Argonne, Illinois 60439. For information about Argonne and its pioneering science and technology programs, see www.anl.gov.

ANL-NSE-19/9

Development of Heat Pipe Reactor Modeling in SAM

prepared by
G. Hu, R. Hu, and L. Zou
Nuclear Science and Engineering Division, Argonne National Laboratory

June 2019

EXECUTIVE SUMMARY

System Analysis Module (SAM) is under development at Argonne National Laboratory as a modern system-level modeling and simulation tool for advanced non-light water reactor safety analyses. It utilizes the object-oriented application framework MOOSE to leverage the modern software environment and advanced numerical methods available in PETSc. The capabilities of SAM are being extended to enable the transient modeling, analysis, and design of various advanced nuclear reactor systems. This report presents the development of new capabilities for modeling the heat pipe type reactor systems.

The need for power at remote locations away from a reliable electrical grid is an important niche for nuclear energy. Heat pipe-cooled fast-spectrum nuclear reactors are well suited for these applications. The key feature of the heat pipe reactors is the use of heat pipes for heat removal from the reactor core. The heat pipe makes use of the phase change of the working fluid and transports a large amount of heat from the evaporator to the condensation end with very small temperature drops. In contrast to the traditional nuclear reactor system that makes use of pumped loop for extracting the thermal power, the heat pipe reactors make use of hundreds of heat pipes for removing the thermal power (including the decay heat) passively. This could potentially significantly improve the reliability and safety of the reactor systems.

The essential part in the analysis of a heat pipe type reactor is the modeling of heat transport inside the heat pipe. The capability of SAM is extended in this work to enable the modeling of the conventional heat pipe. Two alternative modeling options, 2D-RZ Heat conduction and 3D-1D coupling, are developed, which are both based on the assumption that the heat pipe vapor core can be modeled as a superconductor of extremely high thermal conductivity. Both modeling options are verified with a simplified thermal resistance model. The heat pipes are also coupled with the fuel region of a prototype micro reactor under both normal and off-normal conditions. It is confirmed that both modeling options can correctly model the heat transport in the heat-pipe reactors.

Table of Contents

LIST OF FIGURES

LIST OF TABLES

1 Introduction

Over the past few years, the rapidly rising interest in advanced nuclear reactor technology has led to an increased need for the developments and applications of advanced computational tools for modeling and simulation. System Analysis Module (SAM) is being developed at Argonne National Laboratory as a modern system-level modeling and simulation tool for advanced non-light water reactor safety analyses [1]. It utilizes the object-oriented application framework MOOSE [2] to leverage the modern software environment and advanced numerical methods of PETSc [3]. The capabilities of SAM are being extended to enable the transient modeling, analysis, and design of various advanced nuclear reactor systems.

The need for power at remote locations away from a reliable electrical grid is an important niche for nuclear energy. Heat pipe-cooled fast-spectrum nuclear reactors are well suited for these applications [4]. The key part of the heat pipe reactors is the heat pipes used to cool the reactor core. The heat pipe makes use of the phase change of the working fluid and transport a large amount of heat from the evaporator to the condensation end with very small temperature drops [5]. In contrast to the traditional nuclear reactor system that makes use of pumped loop for extracting the thermal power, the heat pipes reactors make use of hundreds of heat pipes for removing the thermal power (including the decay heat) passively. The reliability and safety of the reactor system can be significantly improved. The essential part in the analysis of a heat pipe type reactor is the modeling of heat transport in the heat pipe. The capability of SAM is extended in this work to enable the modeling of the conventional heat pipe.

Two alternative modeling options are proposed, which are both based on the assumption that the heat pipe vapor core can be seen as a superconductor of extremely high thermal conductivity. In the first option, the heat pipe wall, wick, and vapor core are modeled together as an axisymmetric heat structure. The heat is transported into/out the vapor core from the heat pipe wall through heat conduction between the wick and the vapor core. The vapor core is assumed to be have an extremely high thermal conductivity. The heat pipe is then coupled with the reactor core and condenser heat exchanger through the heat pipe outer wall. In the second option, the heat pipe wall and wick are separated from the heat pipe vapor core. The heat pipe wall and wick are modeled as a three-dimensional (3D) heat structure, which can be modeled directly with the reactor core. The heat pipe vapor core is modeled as a one-dimensional (1D) heat line of very high thermal conductivity. The heat pipe wick and the heat pipe vapor core are coupled through a conjugate heat transfer.

This document is structured as follows: Section 2 provides an overview of the heat pipe modeling options in SAM; Section 3 presents the verifications of the heat pipe modeling approaches; Section 4 describes several demonstration simulations for heat-pipe reactors using single-cell and seven-cell models. A brief summary of this work is provided in Section 5.

2 Heat Pipe Modeling

2.1 Introduction

The heat pipe is a very effective device for transmitting heat at high rates through a small cross-sectional area over a long distance but with small temperature drops. The advantages of using a heat pipe over other conventional methods include for example exceptional flexibility, simple construction, easy maintenance, and easy control with no external pumping power.

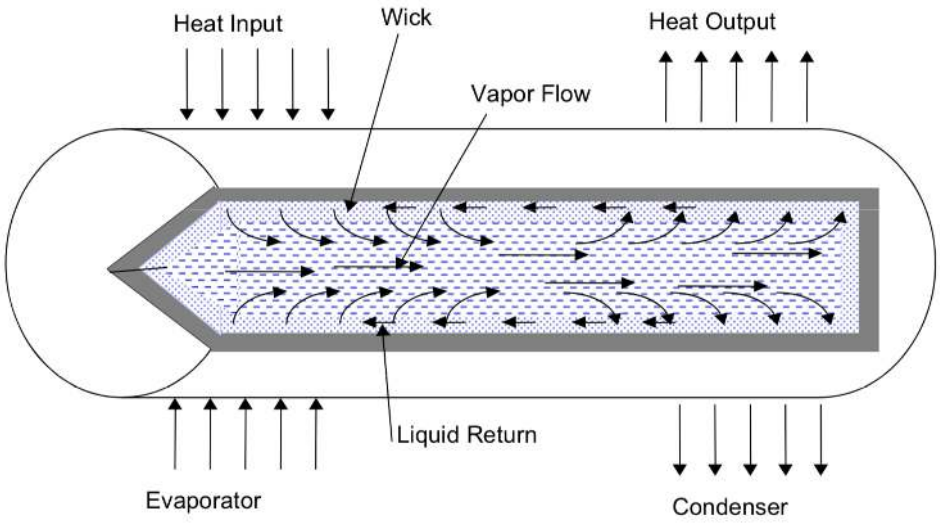

Figure 1: Schematic of a conventional heat pipe showing the principle of operation and circulation of the working fluid

Figure 1 [6] shows a schematic of the conventional heat pipe that shows the principle of operation and circulation of the working fluid. The components of a heat pipe are a sealed container which includes the pipe wall and end caps, a wick structure, and a small amount of the working fluid. The conventional heat pipe contains mainly three parts: evaporator section, adiabatic section, and the condenser section. The external heat is applied to the evaporator section through the pipe wall and wick structure. The external heat vaporizes the working fluid in the wick structure, which increase the vapor pressure in the evaporator region. The vapor pressure then drives the vapor through the adiabatic section to the condenser section. In the condenser section, the vapor condenses and releases its latent heat to the external heat sink through the wick structure and pipe wall. The capillary pressure created by the menisci in the wick drives the condensed fluid back to the evaporator section. This process will continue as long as the capillary pressure is enough to drive the condensed working fluid back to the condenser region.

Heat pipes have been designed with different configurations for different applications, including for example Two-phase closed thermosyphon, Capillary-drive heat pipe, Annular heat pipe, Flat-plate heat pipe, Gas-Loaded heat pipe, and other types [5, 6]. All heat pipes have an evaporator and condenser section. Many heat pipes also have an adiabatic section which separates the evaporator and the condenser sections. The heat pipes can also be classified to a Constant Conductance Heat Pipe (CCHP) and a Variable Conductance Heat Pipe (VCHP). In a conventional heat pipe, the operating temperature is determined by the heat source and heat sink conditions. The conductance of a conventional heat pipe is a nearly constant parameter. The conventional heat pipe is thus a CCHP. In the contrast, the conductance of a VCHP is variable. An example of a VCHP is the Gas-loaded heat pipe, which uses a fixed amount of buffer noncondensible gas to control its

operating temperature. The noncondensible gas forms a barrier to vapor flow and condensation. The overall condenser heat transfer capability is variable and thus provide a variable total conductance, which will control the operating temperature. This report will focus on the conventional capillary-driven heat pipe.

There are various parameters that put limitations on the steady and transient operation of heat pipes. The rate of heat transfer through a heat pipe is subject to several operation limits. The operation limits include, but not limited to, capillary, sonic, entrainment, viscous, and boiling limits. The operation of a heat pipe is limited by the strictest limit among different operation limits Since the vapor flow is not modeled in the current modeling approaches in SAM, the detailed analysis to these operation limits will not be the focus of this report. The detailed analysis of the various operation limits can be found in [5, 6, 7, 8].

2.2 Heat Pipe Modeling Methodology

The heat pipe theory focuses on the fundamental analyses of hydrodynamic and heat transfer processes in the heat pipe. The hydrodynamic theory is usually used to describe the axial pressure drop in the wick structure, the capillary pumping rate, and the vapor flow in the vapor channel. Heat transfer theory is applied to model the heat transfer of heat into and out of the heat pipe. The important physics in the modeling of a heat pipe includes mainly the capillary driving force between the liquid and the vapor interface, the interfacial mass and heat transfer, and the transport of vapor flow in the core of the heat pipe [5].

The thermal fluid phenomena in a heat pipe can be divided into four basic categories: 1) heat conduction in the heat pipe wall; 2) liquid flow and heat transfer in the wick structure; 3) interfacial mass, momentum, and energy transfer in the liquid vapor interface; and 4) vapor flow in the heat pipe core. The heat conduction and the vapor flow are usually modeled as a conjugate heat transfer problem. Various analytical and numerical models, ranging from the simple analytical model to detailed three-dimensional numerical analysis, have been proposed [5]. Of these models, the thermal-resistance model [5] is the simplest one for designing and estimating the operation conditions of a heat pipe. The thermal resistance model will be used in this report to verify the modeling approaches in SAM.

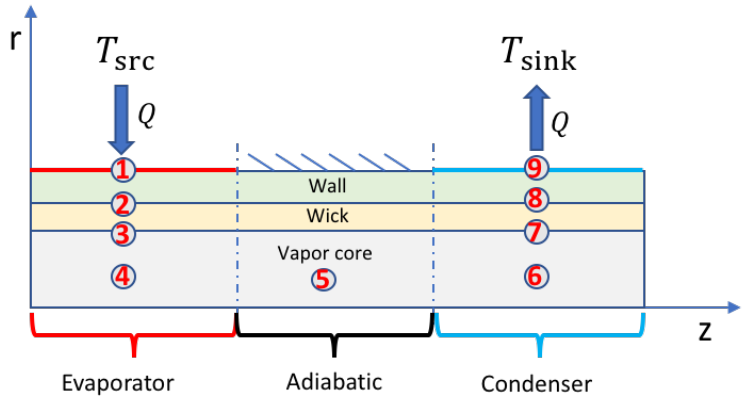

Figure 2: Schematic of a conventional heat pipe

2.2.1 Thermal resistance model

A schematic of the convention heat pipe is shown in Figure 2. For steady-state heat pipe operation analysis, the thermal resistance model is used to provide approximate reference results for verification of SAM models. The thermal resistance model for a conventional heat pipe is shown in Figure 3. The meaning of various location indicator and thermal resistance are listed below Table 1 and Table 2, respectively. Note that Figure 3 also lists the effective wall and wick axial resistance, i.e. R_{19}, which is in practice much larger than the radial resistance and the vapor core axial transport resistance. Thus, R_{19} will be ignored in the following models and analysis.

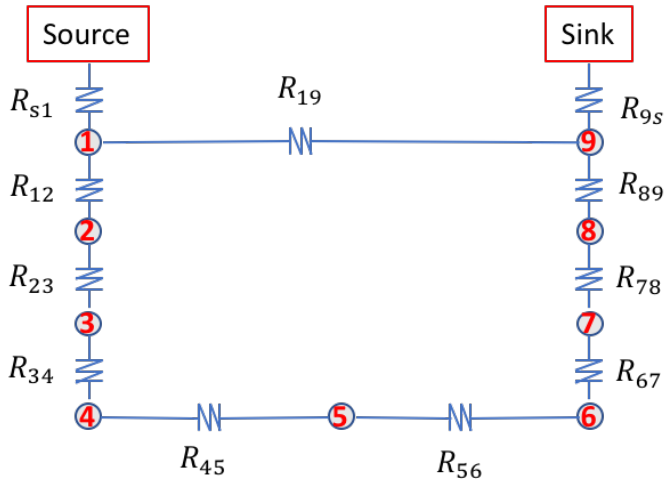

Figure 3: Thermal resistance model for a conventional heat pipe

Table 1: Meaning of different locations in the heat pipe resistance circuit

Location indicator	Average temperature	Meaning
Source	T_{src}	External heat source to the heat pipe
1	T_1	Interface between the heat pipe wall and source in the evaporator region
2	T_2	Interface between the heat pipe wall and wick in the evaporator region
3	T_3	Interface between the heat pipe wick and vapor core in the evaporator region
4	T_4	Center of the vapor core in the evaporator region
5	T_5	Center of the vapor core in the adiabatic region
6	T_6	Center of the vapor core in the condenser region
7	T_7	Interface between the heat pipe vapor core and wick in the condenser region
8	T_8	Interface between the heat pipe wick and wall in the condenser region
9	T_9	Heat pipe container outer wall in the condenser region
Sink	T_{sink}	External heat sink to the heat pipe

Table 2: Meaning of different thermal resistance in the heat pipe resistance circuit

Thermal resistance	Meaning
R_{s1}	External heat source to evaporator outer wall contact resistance
R_{12}	Evaporator wall radial resistance
R_{23}	Evaporator wick radial resistance
R_{34}	Evaporator wick to vapor core (liquid-vapor) interface resistance
R_{45}	Vapor core evaporator-adiabatic axial transport resistance
R_{56}	Vapor core adiabatic-condenser axial transport resistance
R_{67}	Condenser vapor core to wick (vapor-liquid) interface resistance
R_{78}	Condenser wick radial resistance
R_{89}	Condenser wall radial resistance
R_{9s}	Condenser outer wall to external heat sink contact resistance
R_{19}	Effective wall and wick axial resistance

Given the temperature of heat source and heat sink, and the thermal resistance, the heat transport capability is obtained with

$$Q = \frac{T_{\text{src}} - T_{\text{sink}}}{R_{\text{total}}} \tag{2-1}$$

where R_{total} is the total thermal resistance from the heat source to the heat sink ignoring the axial resistance in the wall and wick,

$$R_{\text{total}} = R_{s1} + \sum_{i=1}^{8} R_{i,i+1} + R_{9s} \tag{2-2}$$

Note that the calculation of these thermal resistances will depend on the modeling approaches, which will be discussed in the following section. The average temperatures at locations 1-9 are obtained with

$$T_9 = T_{\text{sink}} + \text{Q} \cdot R_{9s} \tag{2-3}$$

$$T_i = T_{i+1} + Q \cdot R_{i,i+1}, \qquad \text{for } i = 8, 7, \dots, 1 \tag{2-4}$$

2.3 Modeling options in SAM

The main difficulties in modeling the heat pipe are the conjugate interface mass/momentum/energy transfer between the wick and the vapor core, and the vapor flow in the vapor core region. The main approximation for modeling the heat pipe in SAM is that the vapor core can be modeled as a superconductor with a very large thermal conductivity. The heat from the source will be transported to the vapor core from the interface between the wick and the vapor core in the evaporator region, then be conducted axially through the vapor core to the condenser region, and then be transported to wick from the interface between the vapor core and the wick in

the condenser region, and finally be transported to the heat sink. The following two modeling options are proposed:

1. 2D – RZ Heat conduction
2. 3D – 1D coupling

Assuming constant material properties in the wall, wick, and vapor core, the thermal resistances listed in Table 2 can be obtained. Several of these thermal resistances are the same for these 2 modeling options, they are listed in Table 3. The remaining 4 thermal resistances, i.e. R_{34}, R_{45}, R_{56}, and R_{67}, would depend on the modeling options.

Table 3Estimation of common thermal resistances for 3 modeling options

Thermal resistance	Meaning of new variables
$R_{s1} = \frac{1}{A_{s1} h_{s1}}$	A_{s1}: area of the surface between the heat source and heat pipe outer wall in the evaporator region h_{s1}: effective heat transfer coefficient between the heat source and heat pipe outer wall in the evaporator region
$R_{12} = \frac{\log(D_{wall}/D_{wick})}{2\pi \cdot k_{wall} \cdot L_e}$	D_{wall}, D_{wick}: outer diameter of the heat pipe wall and wick k_{wall}: thermal conductivity of the heat pipe wall L_e: length of the evaporator region
$R_{23} = \frac{\log(D_{wick}/D_{vapor})}{2\pi \cdot k_{wick} \cdot L_e}$	D_{wick}, D_{vapor}: outer diameter of the heat pipe wick and vapor core k_{wick}: thermal conductivity of the heat pipe wall L_e: length of the evaporator region
$R_{78} = \frac{\log(D_{wick}/D_{vapor})}{2\pi \cdot k_{wick} \cdot L_c}$	D_{wick}, D_{vapor}: outer diameter of the heat pipe wick and vapor core k_{wick}: thermal conductivity of the heat pipe wall L_c: length of the condenser region
$R_{89} = \frac{\log(D_{wall}/D_{wick})}{2\pi \cdot k_{wall} \cdot L_c}$	D_{wall}, D_{wick}: outer diameter of the heat pipe wall and wick k_{wall}: thermal conductivity of the heat pipe wall L_c: length of the condenser region
$R_{9s} = \frac{1}{A_{9s} h_{9s}}$	A_{9s}: area of the surface between the heat sink and heat pipe outer wall in the condenser region h_{9s}: effective heat transfer coefficient between the heat sink and heat pipe outer wall in the condenser region

2.3.1 Axisymmetric 2D – RZ Heat conduction

In the 2D-RZ heat conduction approach, the heat pipe wall, heat pipe wick, and heat pipe vapor core are modeled as axisymmetric 2D-RZ blocks, with all heat being transported through heat conduction. The wall region is modeled as the normal container material, the is modeled as a solid material using an effective thermal conductivity, and the vapor core is modeled as a superconducting material with an ad-hoc very large thermal conductivity. Figure 4 shows the schematic for an example of the meshed blocks.

Since the wick structure is modeled as a normal heat conduction material, an effective thermal conductivity of the wick structure needs to be provided. The effective thermal conductivity of the wick structure is dependent on both the solid wick material and the working fluid. For liquid metal heat pipes, the high conductivity of the working fluid provides for a high effective conductivity. The effective thermal conductivity can be estimated with the weighted harmonic average [5],

$$k_{wick} = \frac{k_l k_s}{\varphi k_s + (1-\varphi) k_l} \tag{2-5}$$

where the subscripts s and l refers to the solid and liquid phases, φ is the porosity of the wick.

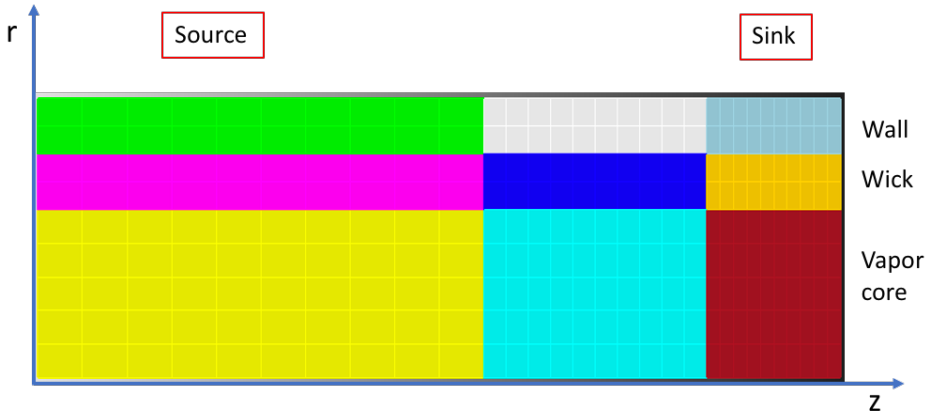

Figure 4 Schematic of the mesh for 2D-RZ heat conduction model

For this option, the 4 thermal resistances, i.e. R_{34}, R_{45}, R_{56}, and R_{67}, can be estimated with

$$R_{34} = \frac{D_{vapor}}{2 \cdot A_{34} \cdot k_{vapor}} \tag{2-6}$$

$$R_{45} = \frac{L_e + L_a}{2 \cdot A_{vapor} \cdot k_{vapor}} \tag{2-7}$$

$$R_{56} = \frac{L_a + L_c}{2 \cdot A_{vapor} \cdot k_{vapor}} \tag{2-8}$$

$$R_{67} = \frac{D_{vapor}}{2 \cdot A_{67} \cdot k_{vapor}} \tag{2-9}$$

where A_{34} is the surface area between the wick and the vapor core in the evaporator region, A_{67} is the surface area between the wick and the vapor core in the condenser region, A_{vapor} is the cross-section area of the vapor core, and k_{vapor} is the effective thermal conductivity of the vapor core.

2.3.2 3D – 1D coupling between heat structure and vapor core

In the 3D – 1D coupling option, the heat pipe wall and wick will be meshed separately from the vapor core. The schematic of the modeling approach is shown in Figure 5. The wall and wick will be modeled as the 3D heat structure while the vapor core will be modeled as a 1D heat structure

representing the heat conduction in a superconducting material. The axial temperature profile of the vapor core is recovered, representing a non-perfect superconductor of a finite but very large thermal conductivity. The 3D heat structure and the vapor core are coupled through convective heat transfer at the wick-vapor core boundaries. Let T_v be the vapor temperature and h_v be the effective heat transfer coefficient between the wick and the vapor core. The boundary condition between the wick and the vapor core is

$$q_w = h_v \cdot (T_w - T_v) \tag{2-10}$$

where T_w and q_w are the wall temperature and wall heat flux at the wick-vapor boundary, respectively. The governing equation for the 1D vapor core is

$$\rho_v C_{pv} \frac{\partial T_v}{\partial t} + k_v \frac{\partial^2 T_v}{\partial z^2} + q_v'''(z) = 0 \tag{2-11}$$

where q_v''' is the volumetric heating source for the vapor core

$$q_v'''(z) = q_w \times a_w \tag{2-12}$$

where a_w is the heated surface area density. Two adiabatic boundary conditions are applied to *(2-11)* at the bottom and top node, which ensures that there is no heat loss in the vapor core region.

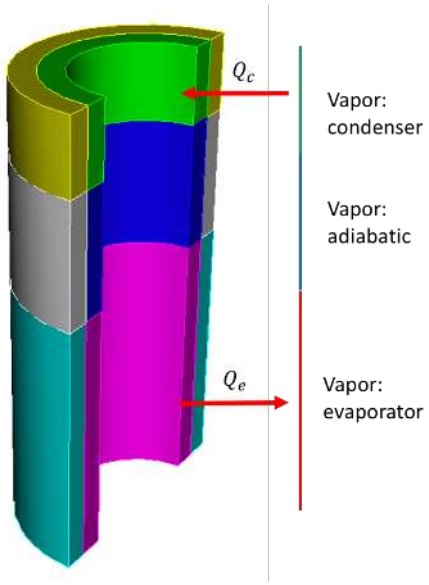

Figure 5: Schematic of the coupling between 3D heat structure with the vapor core

For this option, the 4 thermal resistances, i.e. R_{34}, R_{45}, R_{56}, and R_{67}, can be estimated with

$$R_{34} = \frac{1}{A_{34} \cdot h_v} \tag{2-13}$$

$$R_{45} = \frac{L_e + L_a}{2 \cdot A_{vapor} \cdot k_{vapor}} \tag{2-14}$$

$$R_{56} = \frac{L_a + L_c}{2 \cdot A_{vapor} \cdot k_{vapor}} \tag{2-15}$$

$$R_{67} = \frac{1}{A_{67} \cdot h_v} \tag{2-16}$$

Note that R_{45} and R_{56} are non-zero because of the finite thermal conductivity.

It is noted that the effective heat transfer coefficient between the wick and the vapor core, i.e. h_v, needs to be provided to the 3D-1D modeling option. The effective heat transfer coefficient [5] between the wick and the vapor core is estimated with

$$h_v = \left(\frac{2\alpha}{2-\alpha}\right)\left(\frac{h_{fg}^2}{T_v v_{fg}}\right)\sqrt{\frac{M_v}{2\pi R_u T_v}}\left(1 - \frac{p_v v_{fg}}{2h_{fg}}\right) \tag{2-17}$$

where v_{fg} is the difference in the specific volume of the liquid and vapor phase, α is the empirical term representing the accommodation coefficient, R_u is the universal gas constant, M_v is the molecular weight of the vapor, p_v is the pressure of the vapor, T_v is the temperature of the vapor, h_{fg} is the difference between the specific enthalpy of liquid and gas phase under saturation.

2.3.3 Stability requirement for option 2

The coupling between the 3D heat structure with the vapor core is a conjugate heat transfer problem. The solution of the heat conduction equation in the 3D structure requires the vapor temperature while the solution of the vapor temperature equation requires the wall heat flux at the wick and vapor core boundaries. Since the 3D structure and the vapor core are modeled separately, the coupling scheme is not necessarily stable because of the 1 iteration lag in the calculation of different parts. The stability requirement could be analyzed through an approximate error propagation analysis.

For simplicity, the error analysis will consider only the evaporator region. The boundary condition for the 3D heat structure is

$$k_{wick}\frac{T_0 - T_w}{\Delta r} = h_v(T_w - T_v) \tag{2-18}$$

where T_w represents the wall temperature, T_0 represents the solid temperature in the inner neighboring node of T_w, and Δr represents the mesh size in the radial direction.

The transient governing equation for the average vapor temperature is

$$VC_p\frac{\partial T_v}{\partial t} = q_w \times A_v \tag{2-19}$$

In the limit of a small time step, assuming the variation in T_0 is much smaller than the change in the T_w and T_v, then

$$q_w = h_v\frac{k_{wick}}{k_{wick} + h_v\Delta r}(T_0 - T_v) \tag{2-20}$$

$$\frac{\partial T_v}{\partial t} = \frac{h_v S}{\rho V C_p}\frac{k_{wick}}{k_{wick} + h_v\Delta r}(T_0 - T_v) = \frac{1}{\tau_0}(T_0 - T_v) \tag{2-21}$$

where

$$\tau_0 = \frac{\rho V C_p}{h_v S} \frac{k_{wick} + h_v \Delta r}{k_{wick}} \tag{2-22}$$

Let n specifies the iteration number. Note that the coupling between the 3D heat structure and the vapor core marches in an explicit way, i.e.

$$T_v^{n+1} = T_v^n + \frac{\Delta t}{\tau_0}(T_0 - T_v^n) = \left(1 - \frac{\Delta t}{\tau_0}\right) T_v^n + \frac{\Delta t}{\tau_0} T_0 \tag{2-23}$$

The condition for the coupling scheme to be stable is

$$\left|1 - \frac{\Delta t}{\tau_0}\right| < 1 \tag{2-24}$$

which requires

$$\Delta t \ll \tau_0 \tag{2-25}$$

However, this condition is very strict. For example, in one of the numerical test,

$$k_{wick} = 65, \Delta r = 1.25 \times 10^{-3}, h_v = 10^6, D = 0.06, L = 1.1, S = 0.207$$
$$\rho = 1, C_p = 10^3, V = 3.11 \times 10^{-3} \tag{2-26}$$

which gives $\tau_0 = 3.04 \times 10^{-4}$ s. This τ_0 is too strict for the scheme to be stable.

It is observed that the main parameters that governs stability condition is the total heat capacity of the vapor core, i.e. $\rho V C_p$. For example, by taking $\rho V C_p = 10^4$, τ_0 is increased to $\tau_0 = 0.98$ s, which is reasonable for practical simulations. Since the vapor volume is fixed and the vapor density is usually small, the stability condition requires that the specific heat capacity is large enough. This condition can be justified by the fact that the vapor temperature change is related to the phase change and the latent heat, a significant amount of external heat is required to change the vapor pressure and thus the vapor temperature.

2.4 Advantages and Disadvantages

2.4.1 Option 1: SAM 2D-RZ

This is the simplest modeling option and is implemented as a customized component in SAM. The simulation cost is minimum. The energy conservation is guaranteed, meaning all the heat into the heat pipe from the heat source will be transported out to the heat sink. In this option, the vapor core is solved with the heat pipe wall and wick in a fully implicit way, the stability requiremen on the total heat capacity is less strict. However, there is one free parameter, i.e. the effective thermal conductivity of the vapor core, which is important yet not clearly defined. In general, the effective thermal conductivity of the vapor core has to be very large, e.g. 10^7 W/(m-K) is used in the verification tests. If the effective thermal conductivity is too large, it may introduce a convergence difficulty to the solver, because a very sharp temperature gradient is introduced near the wick and the vapor core boundary. Besides, this option is only used for modeling the heat pipe, all other blocks, e.g. the fuel region in a heat pipe reactor, need to be modeled separately and coupled with the heat pipe.

2.4.2 Option 2: SAM 3D-1D

In this option, the 3D structure may represent not only the heat pipe wall/wick but also all other blocks in a heat pipe reactor. As long as the surfaces between the wick and the vapor core are specified in the mesh, it can be coupled with the 1D vapor core. Similarly, there is one free parameter, i.e. the effective thermal conductivity of the vapor core, which is important yet not clearly defined. Besides, the stability of the coupling scheme puts a requirement on the total heat capacity of the vapor core, as was discussed in the previous section.

3 Verification of Heat Pipe Modeling

3.1 Heat Pipe Model Description

The modeling options introduced in previous chapter are verified with the resistance model. For simplification purposes, all material properties and heat transfer coefficients are assumed to be constant values. The geometry parameters, material properties, and heat transfer coefficients for the tests are listed in Table 4.

Table 4: Geometry parameters and material properties for heat pipe test problems

	Vapor core	Wick	Wall
Outer diameter: m	0.06	0.065	0.070
Density: kg/m^3	1.00	865.00	7670.00
Specific heat capacity: J/kg	1.0×10^6	1200.00	568.72
Thermal conductivity: W/m-K	1.0×10^7	65.00	21.82
	Evaporator	Adiabatic	Condenser
Length: m	1.0	0.5	0.3
Heat transfer coefficients: W/m^2-K	$h_{s1} = h_{ve} = h_{vc} = 10^6$, $h_{9s} = 10^4$		

The following 3 meshes are needed in this test.

- A 2D-RZ Mesh for the wall, wick, and vapor core: wall, wick, and vapor core are specified in different blocks; boundary surfaces between the heat pipe wall and the heat source/sink are specified.
- A 3D Mesh for the wall and wick: wall and wick are specified in different blocks; boundary surfaces between the heat pipe wall and the heat source/sink are specified; the boundary surfaces between the wick and the vapor core are also specified.
- A 1D mesh for the vapor core.

3.2 Verification with Resistance Model

3.2.1 Test 1

In this test, the source and sink temperature are given as $T_{\text{src}} = 900$ K and $T_{\text{sink}} = 600$ K, respectively. The objective is to evaluate the heat transport capacity and the average temperature at different locations. All 3 modeling options are tested, and the steady-state results are analyzed below. Figure 6 shows the comparison of average temperature at different locations from SAM prediction and the resistance model, and the comparison of the heat transport capacity (i.e. Q in the figure) from SAM prediction and the resistance model. Additionally, Table 5 lists quantitively the comparison for different modeling options. As is indicated by the results, the SAM prediction matches the resistance model very well. Note that there are differences in the prediction results from different modeling options, this is due to the difference in the thermal resistances related to the vapor core, i.e. R_{34}, R_{45}, R_{56}, and R_{67}.

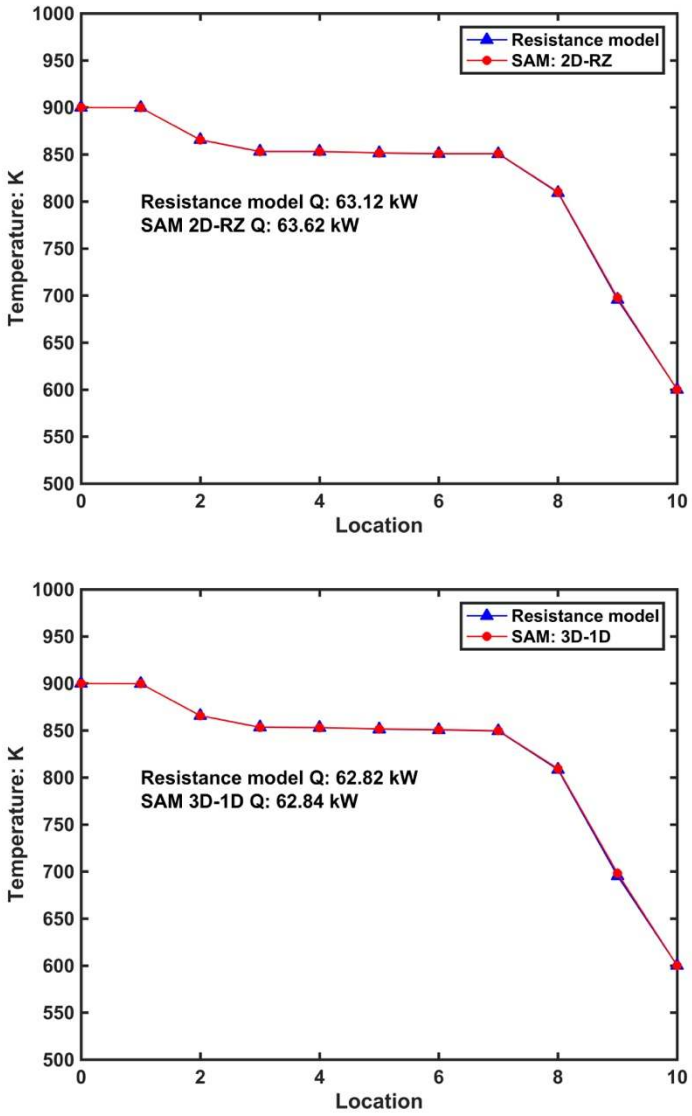

Figure 6: Heat pipe steady-state verification results for Test 1: Option 1 (SAM 2D-RZ, top), and Option 2 (SAM 3D-1D, bottom)

Since both option 1 and option 2 predict the axial profile of the vapor temperature, the results are shown in Figure 7. The axial profile of the vapor temperature is reasonable. In the evaporator region, the vapor temperature drops quadratically due to the heat input from the wall; in the adiabatic region, the vapor temperature drops linearly, since there is not heat input in this region; and in the condenser region, the vapor temperature drops also quadratically due to the heat output to the wall. At the bottom and top end, the temperature gradient is zero, which represents that there is no heat loss from the bottom and top of the heat pipe. The total temperature drop from the vapor core bottom to the vapor core top is proportional to the ratio of the heat transport capacity to the effective thermal conductivity. Note that there is a bias between the vapor temperature from 2D-RZ model and the 3D-1D model. Again, this is because of the thermal resistances difference in these two options.

Table 5: Heat pipe steady-state verification results

	2D-RZ			3D-1D		
	Res.	SAM	Error	Res.	SAM	Error
Q: kW	63.12	63.62	0.79%	62.82	62.84	0.03%
T1: K	899.71	899.71	0.00%	899.71	899.71	0.00%
T2: K	865.59	865.43	-0.02%	865.76	865.64	-0.01%
T3: K	853.22	853.01	-0.03%	853.45	853.29	-0.02%
T4: K	853.22	853.01	-0.03%	853.11	852.95	-0.02%
T5: K	851.55	851.69	0.02%	851.45	851.64	0.02%
T6: K	850.65	850.90	0.03%	850.56	850.86	0.04%
T7: K	850.65	850.90	0.03%	849.45	849.75	0.04%
T8: K	809.41	810.10	0.09%	808.41	809.42	0.13%
T9: K	695.68	697.54	0.27%	695.22	698.15	0.42%

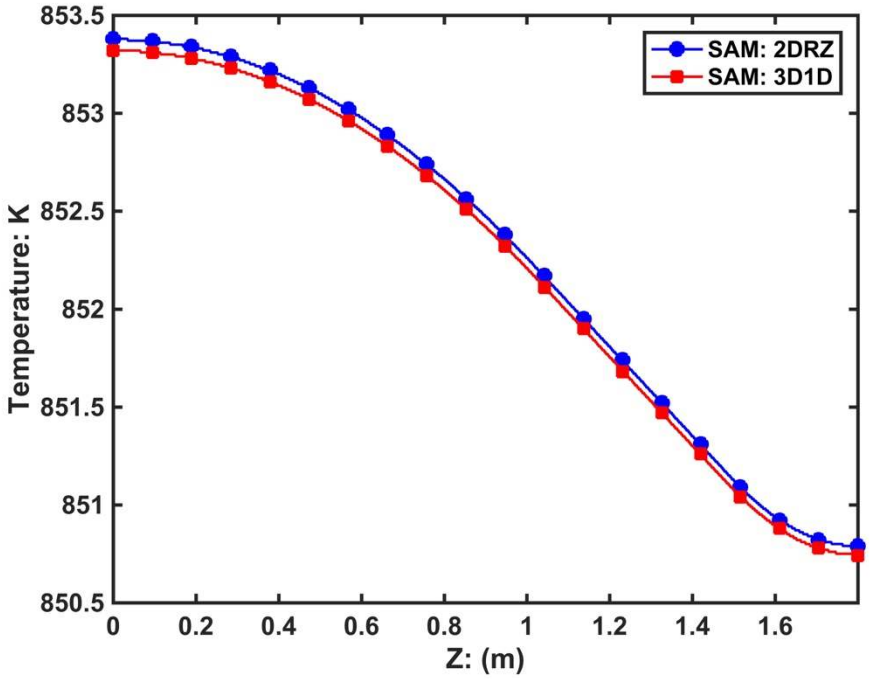

Figure 7: Axial profile of heat pipe vapor temperature at steady-state

3.2.2 Test 2

This test is aimed to study the heat transport capability of the heat pipe as a function of the heat source temperature or the temperature difference between the heat source and heat sink. The geometry parameters, material properties, and the heat transfer coefficients are the same as the Test 1. The heat sink temperature is fixed at $T_{\text{sink}} = 600$ K. The heat source temperature is varied from 700 K to 1400 K. The heat transport capacity is calculated with different modeling options. The results are shown in Figure 8. It is seen that the SAM predictions of the heat transport capacity at various heat source temperature match the resistance model very well. Note that the heat transport capacity is a linear function of the heat source temperature, because of the constant

material properties and heat transfer coefficients. In other words, the total conductance of the heat pipe is constant.

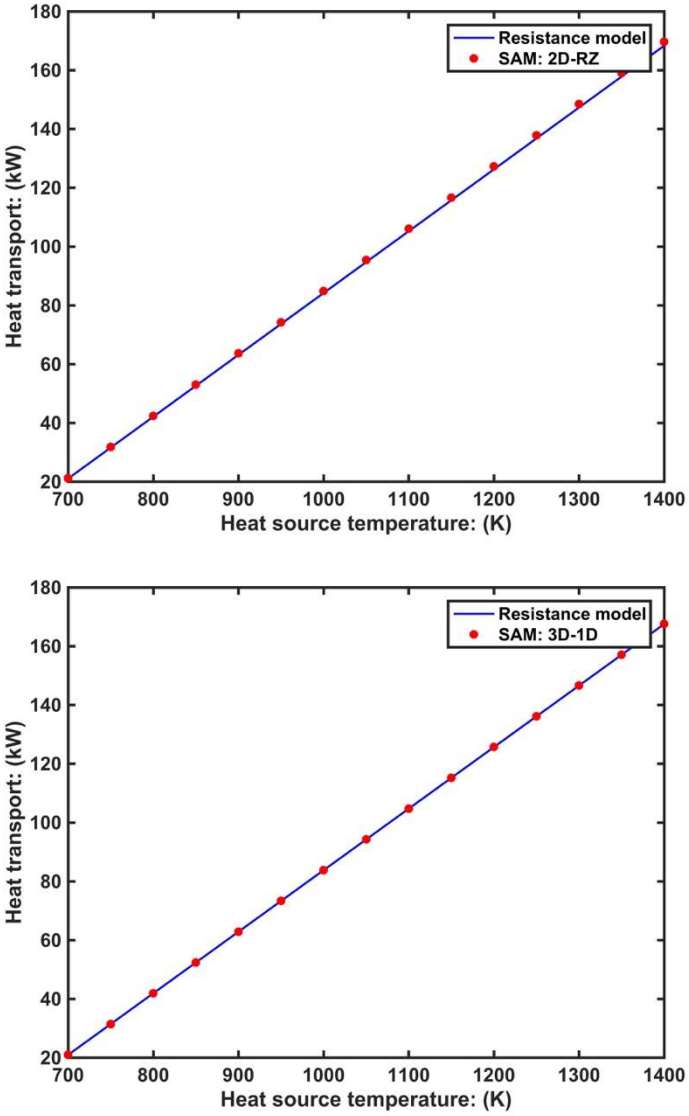

Figure 8: Heat pipe steady-state verification results for Test 2

4 Demonstration of Heat Pipe Reactor Modeling

4.1 Introduction to Heat Pipe Reactors

The need for power at remote locations away from a reliable electrical grid is an important niche for nuclear energy [4]. Nuclear energy has potential applications at strategic defense locations, theaters of battle, remote communities, and emergency locations. Heat-pipe-cooled fast-spectrum nuclear reactors have been identified as a candidate for these applications. Heat pipe reactors are perfectly suited for mobile applications because of their nature. A heat pipe reactor is inherently simpler, smaller, and more reliable than the "traditional" reactors. The key part of the heat pipe reactors is the heat pipes used to cool the reactor core.

As discussed, the heat pipe makes use of the phase change of the working fluid and transport a large amount of heat from the evaporator to the condensation end with very small temperature drops. This feature makes the heat pipe an ideal means to extract thermal power from a nuclear reactor. In contrast to the traditional nuclear reactor system that makes use of pumped loop for extracting the thermal power, the heat pipes reactors make use of hundreds of heat pipes for removing the thermal power (including the decay heat) passively [4]. The reliability and safety of the reactor system can be significantly improved.

This Section presents the new heat pipe modeling capabilities of SAM in the analysis of a made-up heat pipe reactor resign.

4.2 Model Description

The heat pipe modeling approaches have been demonstrated with a single-cell model and a multi-cells model for a heat pipe reactor. The main objective is to evaluate the steady-state operation state of the heat pipe reactor. As is discussed in the previous chapters, both Option 1 and Option 2 will be applied to the single-cell and multi-cells model. For demonstration purposes, made-up dimensions and material properties will be used in the following tests. The working fluid for the heat pipe is assumed to be sodium.

Table 6: Geometry parameters for heat pipe single fuel cell

	Vapor core	HP Wick	HP Wall	Fuel	Hex can	
Inner Radius: m	0	0.015	0.016	0.017	0.0288675	
Outer Radius: m	0.015	0.016	0.017	0.0288675	0.0311769	
	Support plate	Bottom reflector	Fuel	Top reflector	HP Adiabatic	HP Condenser
Height: m	0.05	0.15	1.00	0.15	0.40	0.30
Top location: m	0.05	0.20	1.20	1.35	1.75	2.05

The schematic for the single-cell model is shown in Figure 9. The model is for one heat pipe fuel cell for the axial region of neutronic importance plus the complete heat pipe wall and wick. The model starts with the core support plate and ends at the top of the heat pipe. It consists of Support plate, Bottom reflector, Fuel, Top reflector, Hex can, HP Wall, and HP Wick [4]. Note that the structure details surround the heat pipe adiabatic and condenser regions are ignored. The geometry parameters are listed in Table 6. The total heat pipe length is 2.0 m. The 7-cells model is created based on the single-cell model. The schematic of the 7-cells model is shown in Figure 10.

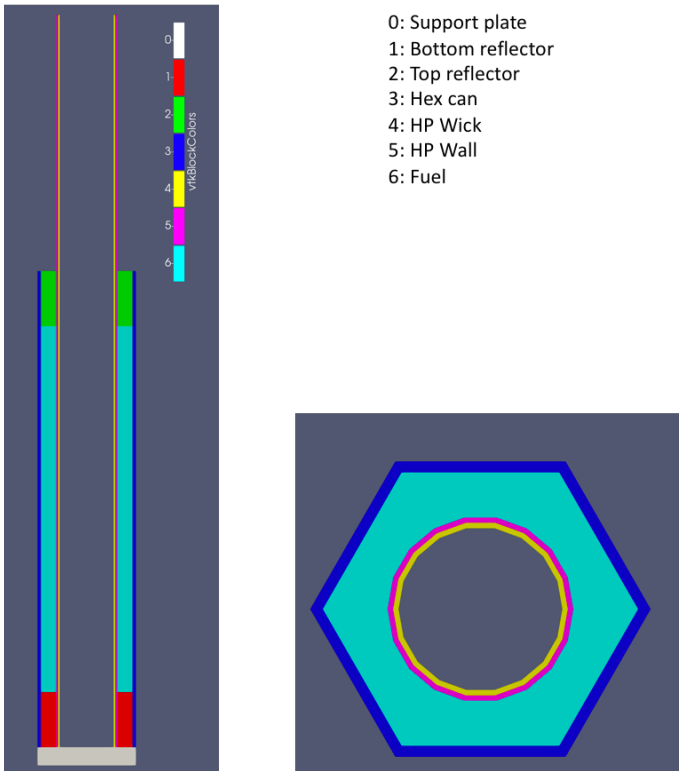

Figure 9: Schematic of the heat pipe reactor single-cell model. Radial dimension is scaled by 5 times.

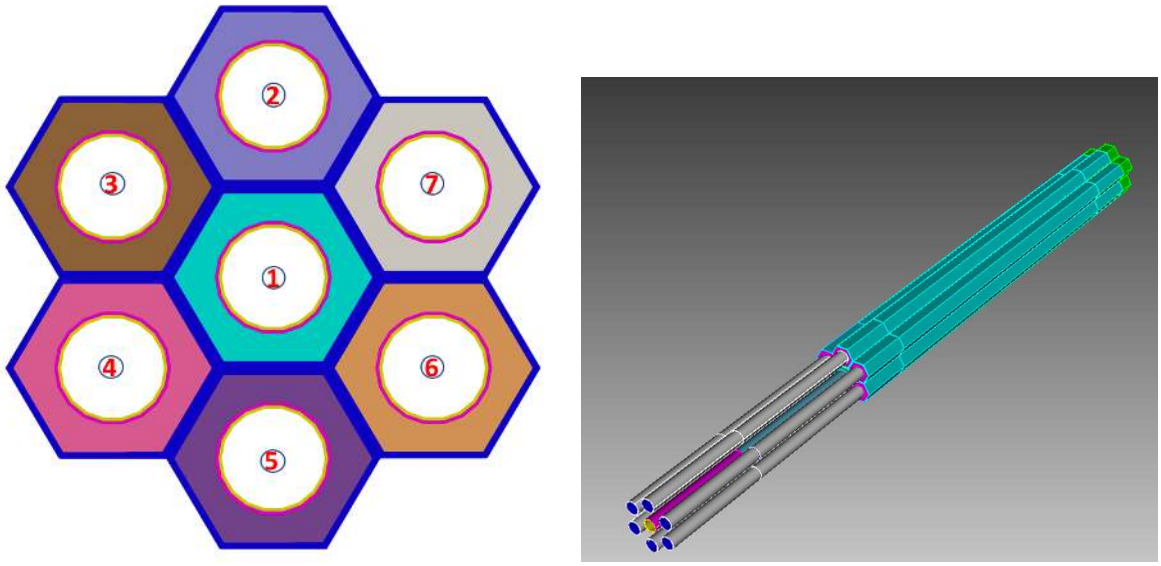

Figure 10: Schematic of the heat pipe reactor 7-cells model.

4.3 Demonstration with the Single-Cell Model

For simplification and demonstration purposes, material properties are assumed to be constant values. The effective heat transfer coefficient between the wick to the vapor core and thermal

conductivity of the wick are estimated with Eq. *(2-17)* and Eq. *(2-5)*. In this demonstration test, the operating temperature for the vapor core is about 800 K, which is used to estimate the properties of the working fluid, which is assumed to be sodium [9]. At $T_v = 800$ K, the related thermal properties of the working fluid are taken as $v_{vg} = 291.6\ \mathrm{m^3/kg}$, $h_{fg} = 4.197 \times 10^6\ \mathrm{J/kg}$. The empirical parameter α is taken to be unity. The remaining parameter is the vapor pressure, which is taken as $p_v = 10^4$ Pa. Thus, the effective heat transfer coefficient between the wick and the vapor core is estimated to be

$$h_v \approx \left(\frac{2\alpha}{2-\alpha}\right)\left(\frac{h_{fg}^2}{T_v v_{fg}}\right)\sqrt{\frac{M_v}{2\pi R_u T_v}}\left(1-\frac{p_v v_{fg}}{2h_{fg}}\right) = 2.34 \times 10^6\ \mathrm{W/m^2K} \qquad (4\text{-}1)$$

As for the effective thermal conductivity of the wick, $k_l = 66.98\ \mathrm{W/mK}$, $k_s = 21.82\ \mathrm{W/mK}$, and $\varphi = 0.8$, which gives

$$k_{wick} = \frac{k_l k_s}{\varphi k_s + (1-\varphi)k_l} = 47.37\ \mathrm{W/(m\ K)} \qquad (4\text{-}2)$$

A complete list of the material properties is given in Table 7.

Table 7: Material properties for heat pipe reactor fuel cell

	Density (kg/m)	Specific heat capacity (J/kg)	Thermal conductivity (W/m-K)
Support plate	7670	568.72	21.82
Reflector	6530	278.0	23.0
Fuel	1685	337.47	19.983
Hex can	7670	568.72	21.82
HP Wall	7670	568.72	21.82
HP Wick	865	1200.0	47.37

The heating power for the single fuel cell is taken as $Q = 24$ kW. A chopped cosine axial power profile is used with an axial peaking factor of 1.2. The simulation is starting with an initial temperature of 600 K in all regions and continuing to reach the steady-state. Figure 11 shows the history of the average temperature at different regions.

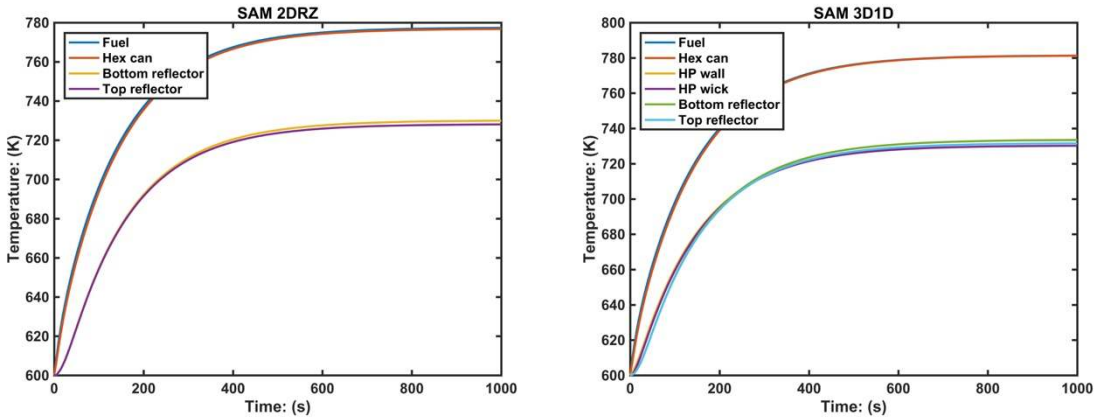

Figure 11: Transient average temperature at different regions for the single-cell model for Option 1 (left, SAM 2D-RZ) and Option 2 (right, SAM 3D-1D)

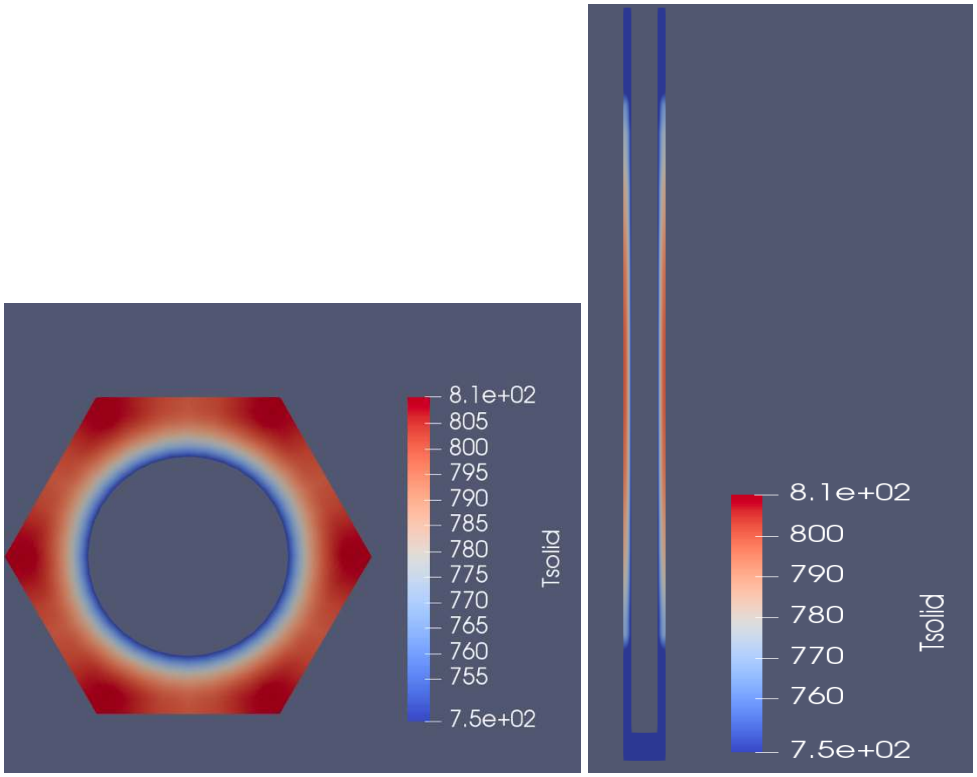

Figure 12: Solid temperature for the single-cell model.

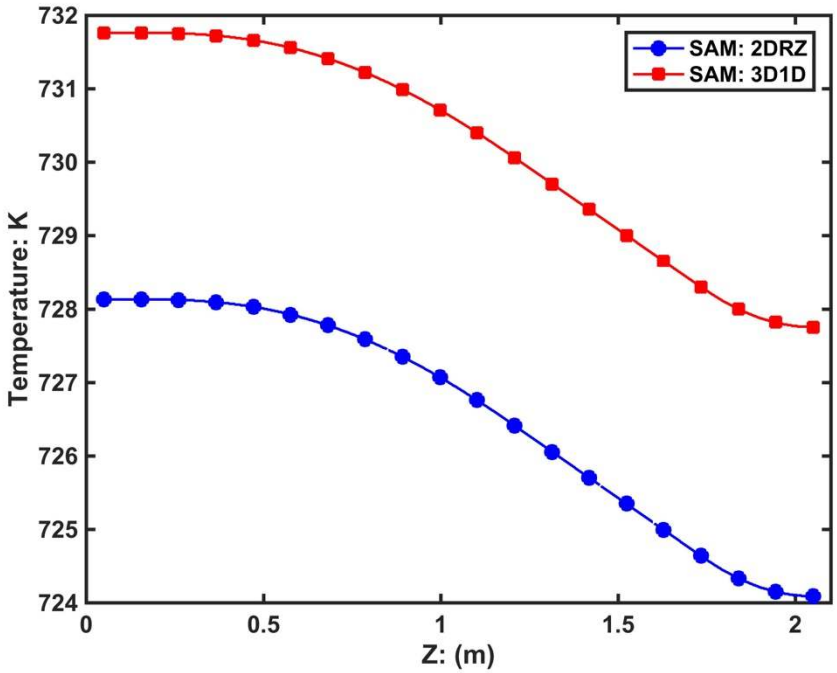

Figure 13: Vapor temperature for the single-cell model.

Figure 12 and Figure 13 show the temperature in the heat structure and in the vapor core, respectively. Both the solid temperature and vapor temperature are reasonable and physical. The gradient of the vapor temperature gradient at the bottom and top side of the heat pipe are zero, representing that there is not heat loss at these boundaries. Note that there is a bias in the vapor temperature between Option 1 and Option 2, which is caused by the different thermal resistance in the vapor core and in the wick to vapor core interface. This difference can be removed if an anisotropic thermal conductivity is available in Option 1 for the vapor core.

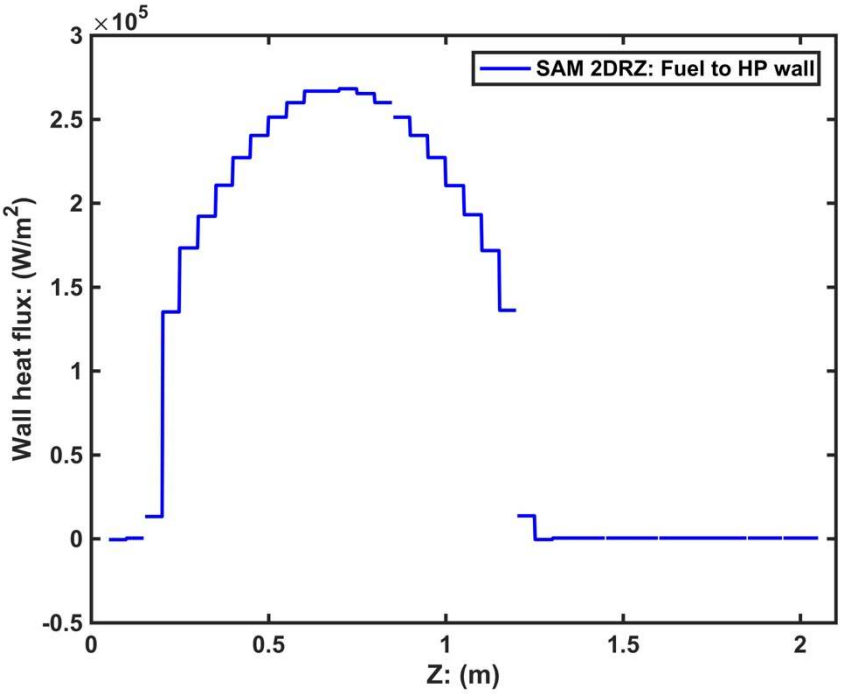

Figure 14: Axial profile of wall heat flux from the fuel to the heat pipe wall for SAM 2D-RZ model.

The wall heat flux from the fuel to the heat pipe wall is used in the SAM 2D-RZ modeling option to couple the heat structure with the heat pipe. The axial profile of the wall heat flux is shown in Figure 14. Similarly, the wall heat flux from the heat pipe wick to the vapor core is used in the SAM 3D-1D modeling option to couple the heat pipe wick with the vapor core. The axial profile of this wall heat flux is shown in Figure 15. The wall heat flux has a cosine profile in the fuel region (from 0.2 m to 1.2 m), which is consistent with the given power profile in the fuel. Note that Figure 15 shows also the wall heat flux in the adiabatic region and condenser region. In the adiabatic region, there is negligible wall heat flux between the heat pipe wick and the vapor core; while in the condenser region, the wall heat flux is negative, representing that the heat is transported from the vapor core to the condenser. Note that the wall heat flux is calculated as a layered average in the boundary, it has piecewise constant values in the different layers.

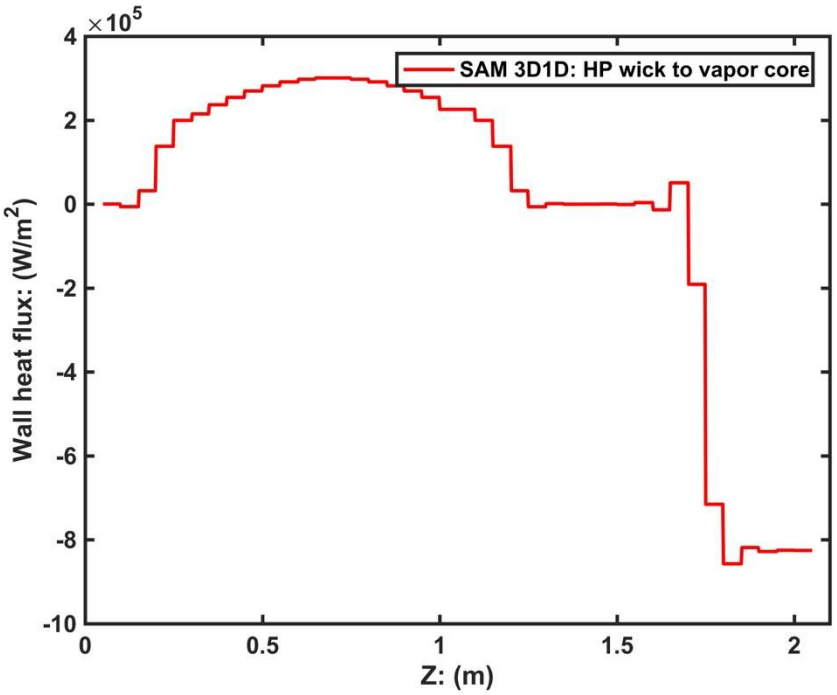

Figure 15: Axial profile of wall heat flux from the heat pipe wick to the vapor core for SAM 3D-1D model.

4.4 Demonstration with the 7-Cells model

The setup for the 7-cells model is similar to the single-cell model. For simplification purposes, the boundary conditions for different fuel cells are the same unless otherwise mentioned. In this demonstration, 2 tests are performed. For these 2 tests, all 7 fuel cells have the same heating power, i.e. $Q = 24$ kW. In the first test (Test 1), all 7 heat pipes are assumed to be working. Due to the symmetry, the operating and temperature profile in different fuel cells should be identical. In the second test (Test 2), the central heat pipe (HP #1) is assumed to be failed, the heat in this fuel cell would be transported out radially to the other 6 fuel cells. The symmetry in the other 6 heat pipes is maintained. Because of the failure of the HP #1, the other 6 heat pipes will work at a higher vapor temperature.

The simulation is starting with an initial temperature of 600 K in all regions and continuing to reach the steady-state. Figure 16 shows the history of the average temperature at different regions. The current simulation stops at 1000 s, at which the system has reached the steady state.

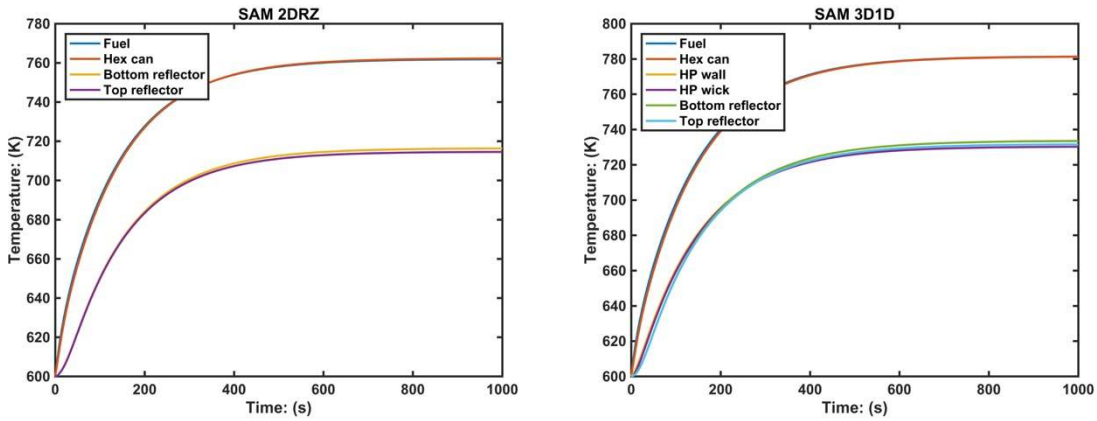

Figure 16: Transient average temperature at different regions for the 7-cells model for SAM 2D-RZ (left) and SAM 3D-1D (right)

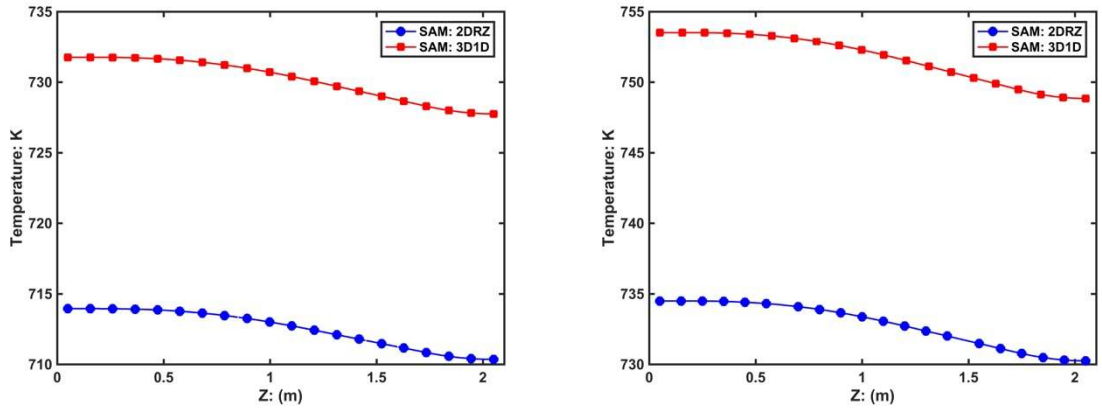

Figure 17: Axial vapor temperature of HP #2 for Test 1 (left) and Test 2 (right).

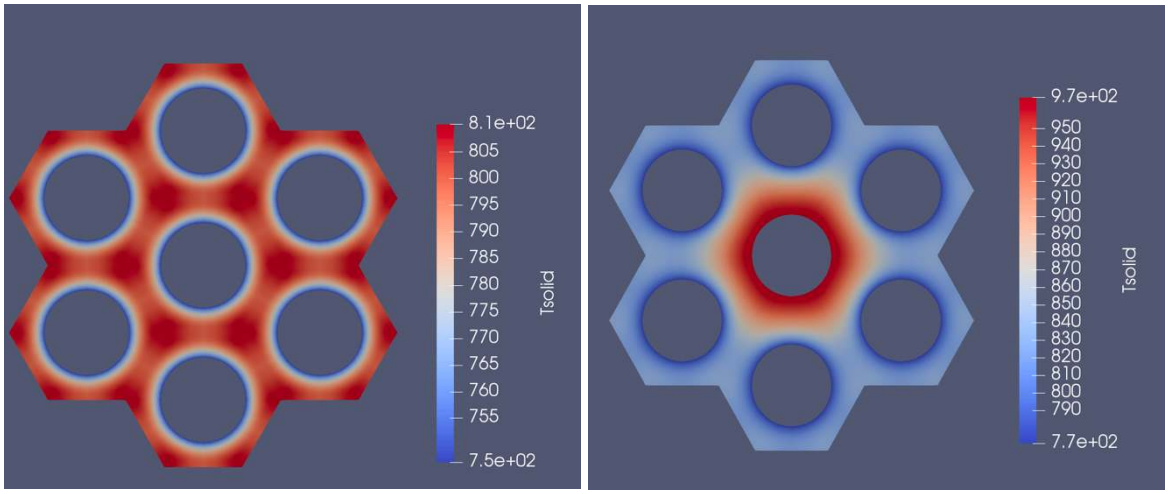

Figure 18: Radial temperature profile for the 7-cells model. for Test 1 (left) and Test 2(right).

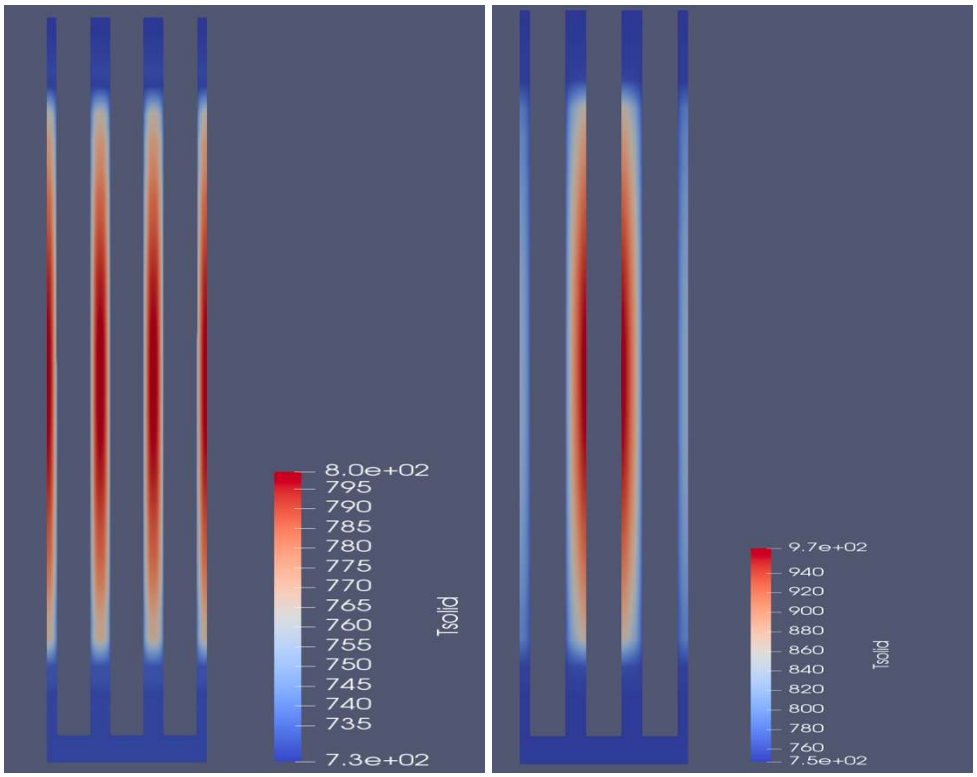

Figure 19: Axal temperature profile for the 7-cells model. Left (Test 1); right (Test 2)

The steady-state simulation results are shown in Figure 17 - Figure 19. Figure 17 shows the axial profile of the vapor temperature in HP #2 for different tests and different modeling options. Figure 18 and Figure 19 shows the radial and axial cross-sectional temperature distribution in the heat structure. The simulation results from SAM 2D-RZ option are similar to the SAM 3D-1D option, except that there is a bias in the solid and vapor temperature due to the difference in the thermal resistance related to the heat pipe. Again, this difference can be removed if an anisotropic thermal conductivity is available in Option 1 for the vapor core.

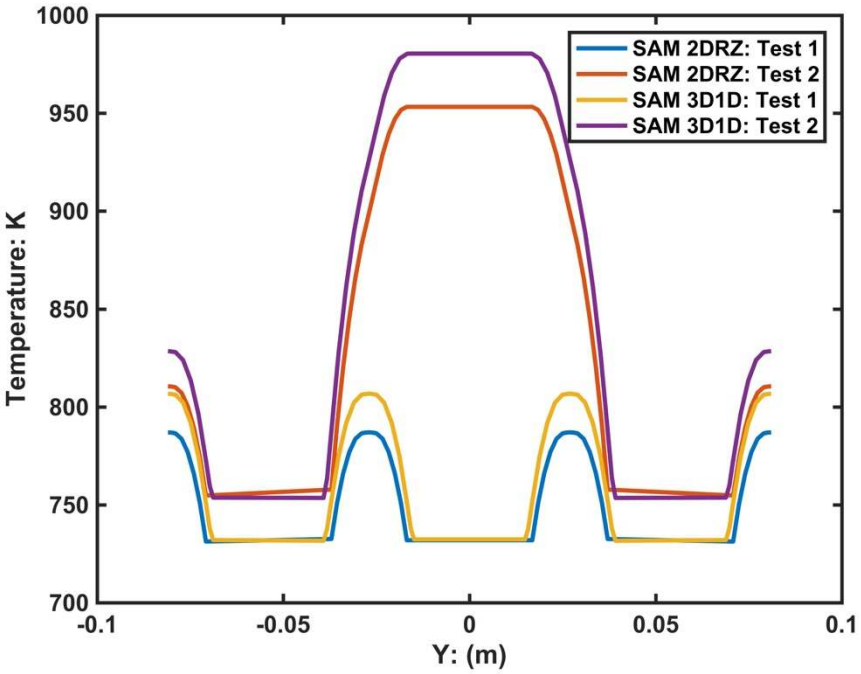

Figure 20: Solid temperature along the Y-axis for the 7-cells model.

In Test 1, since the 7 heat pipes and fuel cells have the same physical and boundary conditions, the operation temperatures in the 7 cells are identical. In Test 2, the central heat pipe (HP #1) is assumed to be failed, the heat in that fuel cell is transported out radially to the other 6 fuel cells. A temperature gradient is formed between cell #1 and the other 6 cells, which gives a much higher fuel temperature in cell #1. A detailed comparison in the solid temperature in shown in Figure 20, in which the solid temperature along the Y-axis at the fuel mid-plane (i.e. $z = 0.7$ m) is presented. The failure of the local heat pipe brings in a local peak in the fuel temperature around that heat pipe. Note that the inter-assembly gap is ignored in the current model, which would need to be considered to predict the local peak more accurately.

5 Summary

Because of the increasing interests in heat-pipe type micro-reactors, the capability of SAM has been extended in this work to enable the modeling of the conventional heat pipe and the heat pipe type reactor. Two modeling options are developed for the analysis of the conventional heat pipe, depending on how the heat is transported between the heat pipe wick and heat pipe vapor core. The essential idea behind these two options is that the vapor core of the heat pipe can be simulated as a superconductor of an extremely high thermal conductivity. Both modeling options are designed such that there is no heat loss in the heat pipe. The proposed modeling options are verified with the classical thermal resistance model. For both modeling options, the temperature at different locations and the heat transport capacity of the heat pipe from the prediction agree very well with the thermal resistance model.

The new capability has also been demonstrated by coupling the heat pipe with the fuel region of a prototype micro reactor. The demonstration is performed at first with a single fuel cell and then 7 fuel cells of the micro reactor. The demonstration with the 7 cells model shows that the new capability can be applied to the analysis of the whole reactor core, which contains hundreds of fuel cells and heat pipes. The simulation results for both modeling options are reasonable. In the demonstration with 7 fuel cells, one test was performed to assess the working condition of the reactor under the condition of a single heat pipe failure. The prediction shows that the failure of a single heat pipe causes a local peak in the fuel temperature, where the peaking factor is mainly determined by the inter-assembly heat transfer characteristic of the reactor.

It should be noted that the proposed modeling options have limitations and require future improvements. The fluid fields, such as velocity and pressure, of the vapor core are missing. The proposed modeling options are not able to predict the heat transport limits and transient behavior of the heat pipe. These limitations are caused by the idea that the vapor core is modeled as a superconductor instead of a fluid flow. Nonetheless, some heat transport limits can be evaluated based on the calculated temperature distributions in the vapor core. It should also be noted that the primary goal of the developed heat pipe modeling capability is to enable the transient safety analyses of the heat-pipe-type reactor systems, not to design a heat pipe.

Acknowledgement

The authors sincerely thank Mr. Joseph Kelly at U.S. Nuclear Regulatory Commission for the fruitful discussions throughout the work and the valuable comments of the report.

This report was prepared as an account of work sponsored by an agency of the U.S. Government. Neither the U.S. Government nor any agency thereof, nor any of their employees, makes any warranty, expressed or implied, or assumes any legal liability or responsibility for any third party's use, or the results of such use, of any information, apparatus, product, or process disclosed in this report, or represents that its use by such third party would not infringe privately owned rights. The views expressed in this paper are not necessarily those of the U.S. Nuclear Regulatory Commission.

Reference:

[1] Hu, R., *SAM Theory Manual*, Nuclear Engineering Division, Argonne National Laboratory, ANL/NE-17/4, Argonne, IL, March, 2017.

[2] Gaston, D., Newman, C., Hansen, G., Lebrun-Grandi'E, D., *MOOSE: A Parallel Computational Framework for Coupled Systems of Nonlinear Equations*, *Nuclear Engineering and Design*, 239, p. 1768–1778, 2009.

[3] Balay, S., et al, *PETSc Users Manual: Revision 3.10*. No. ANL-95/11 Rev 3.10. Argonne National Laboratory, 2018.

[4] Mcclure, Patrick Ray, David Irvin Poston, Venkateswara Rao Dasari, and Robert Stowers Reid. *Design of megawatt power level heat pipe reactors*. No. LA-UR-15-28840. Los Alamos National Lab.(LANL), Los Alamos, NM (United States), 2015.

[5] Faghri, Amir. *Heat pipe science and technology*. Global Digital Press, 1995.

[6] Ku, J., *Introduction to heat pipes,* Thermal and Fluid Analysis Workshop, 2015

[7] Lee, Ho Sung. *Thermal design: heat sinks, thermoelectrics, heat pipes, compact heat exchangers, and solar cells*. John Wiley & Sons, 2010.

[8] Dincer, Ibrahim, and Mehmet Kanoglu. *Refrigeration systems and applications*. Vol. 2. New York: Wiley, 2010.

[9] Fink, J. K., and L. Leibowitz. *Thermodynamic and transport properties of sodium liquid and vapor*. No. ANL--RE-95/2. Argonne National Laboratory, 1995

Nuclear Science and Engineering Division
Argonne National Laboratory
9700 South Cass Avenue, Bldg. 208
Argonne, IL 60439

www.anl.gov

Argonne National Laboratory is a U.S. Department of Energy laboratory managed by UChicago Argonne, LLC